Statistical analysis

All data are presented in mean and SE values. Unpaired t tests were used to compare the parameters of the baroreflex dynamic and static characteristics between the control and CHF groups [13]. To compare the transfer functions between the two groups, we arbitrarily selected the dynamic gain values at 0.01, 0.1, and 1 Hz ($G_{0.01}$, $G_{0.1}$, and G_1). For the step response relating to the neural arc transfer function, the negative peak response (S_{peak}), the time to the negative peak (T_{peak}), the value of the step response at 10 s (S_{10}), the steady-state response at 50 s (S_{50}), and the ratio of the peak response to the steady-state response (S_{peak}/S_{50}) were calculated. For the step response relating to the peripheral arc, total baroreflex, or HR control, an initial slope of the response was calculated (see Appendix 2) in addition to S_{50}. Differences were considered significant when $P < 0.05$.

Simulation study

Once the open-loop dynamic and static characteristics of a system are both identified, closed-loop system responses can be simulated [14–16]. To compare closed-loop behavior of the carotid sinus baroreflex between control and CHF conditions, step inputs ranging from −10 to −60 mmHg were applied as exogenous disturbances, and resulting AP responses were simulated. Percent recovery was calculated as the magnitude of steady-state AP recovery relative to the size of step disturbance. The initial slope for the recovery response was also calculated (see Appendix 2).

Results

Postmortem examination confirmed that the left ventricular free wall was reduced to a membrane-like scar in the CHF group. Biventricular weights, both absolute and relative to body weight, were significantly greater in the CHF than in the control group (Table 1). The central venous pressure was significantly higher and the baseline AP and HR were significantly lower in the CHF group. Although the duration after myocardial infarction ranged from 100 to 200 days in the CHF group, there was no significant correlation between the duration and biventricular weight ($y = 0.0012x + 2.53$, $r^2 = 0.035$, $P = 0.72$, x duration in days, y biventricular weight in grams per kilogram) or between the duration and central venous pressure ($y = -0.013x + 7.5$, $r^2 = 0.07$, $P = 0.58$, x duration in days, y central venous pressure in millmeters of mercury).

Typical experimental recordings obtained from a control rat are shown in Fig. 1a. m-SNA indicates a 2-s moving averaged signal of SNA. In the dynamic input protocol, CSP was changed dynamically according to a GWN signal. m-SNA varied dynamically in response to the CSP perturbation. Although AP changed dynamically, the AP variation seemed more sluggish than the SNA variation. Changes in HR were less obvious from the time series data. In the static input protocol, a stepwise increase in CSP decreased m-SNA, AP, and HR. The noise level of SNA obtained after the intravenous administration of hexamethonium bromide was set at zero. Because of the normalization procedure, m-SNA during the last 10 s at CSP of 60 mmHg approximated 100%. Figure 1b represents CSP and SNA signals sampled at 200 Hz during the dynamic input protocol. High CSP inputs suppressed SNA to a noise level.

Typical experimental recordings obtained from a CHF rat are shown in Fig. 2a. In the dynamic input protocol, CSP was changed dynamically according to a GWN signal. Although m-SNA varied dynamically in response to the CSP perturbation, changes in AP and HR were not obvious from the time series data. In the static input protocol, a stepwise increase in CSP decreased m-SNA, AP, and HR. The magnitudes of the responses in m-SNA, AP, and HR seem smaller than those in the control rat. Figure 2b represents CSP and SNA signals sampled at 200 Hz during the dynamic input protocol. High CSP inputs suppressed SNA to a noise level.

Dynamic characteristics of the carotid sinus baroreflex

Figure 3 summarizes the open-loop dynamic characteristics of the carotid sinus baroreflex averaged for the control

Table 1 Age, body weight, biventricular weight, central venous pressure, mean arterial pressure, and heart rate of the normal control and chronic heart failure (CHF) rats

	Control ($n = 12$)	CHF ($n = 7$)	P value
Age at experiment (weeks)	24 ± 3	30 ± 3	0.237
Body weight (g)	565 ± 28	538 ± 19	0.474
Biventricular weight (g)	1.16 ± 0.04	1.45 ± 0.08**	0.002
Biventricular weight (g kg body weight^{-1})	2.05 ± 0.06	2.71 ± 0.13**	<0.001
Central venous pressure (mmHg)	2.0 ± 0.2	5.4 ± 0.9**	<0.001
Mean arterial pressure (mmHg)	134 ± 4	121 ± 4*	0.037
Heart rate (beats min^{-1})	414 ± 11	350 ± 12**	0.001

Data are presented as mean ± SE

** $P < 0.01$ and * $P < 0.05$ by unpaired t test

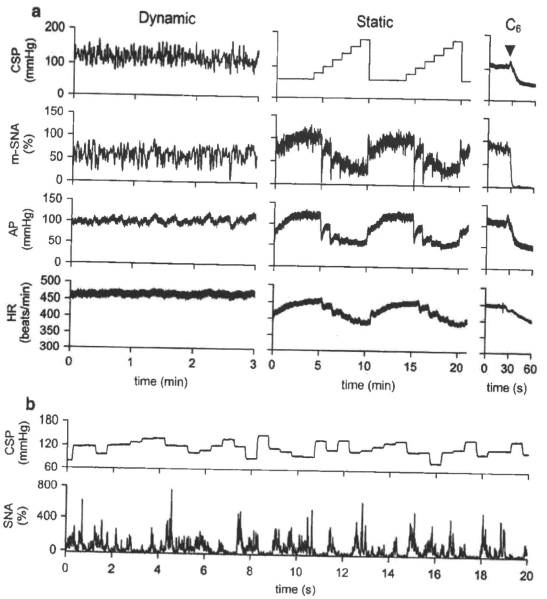

Fig. 1 **a** Typical recordings (10-Hz decimated data) of carotid sinus pressure (CSP), 2-s moving averaged sympathetic nerve activity (m-SNA), arterial pressure (AP), and heart rate (HR) obtained from a control rat. In the dynamic protocol, CSP was changed according to a Gaussian white noise signal. In the static protocol, CSP was increased from 60 to 180 mmHg. Hexamethonium bromide (C_6) was administered intravenously at the end of the experiment (*arrowheads*). The noise level of the nerve activity recorded after C_6 administration was assigned 0%, while the m-SNA value averaged for the last 10 s at CSP of 60 mmHg was assigned 100%. **b** CSP and SNA sampled at 200 Hz during the dynamic input protocol

and CHF rats. The neural arc transfer function from CSP to SNA showed derivative characteristics (Fig. 3a). $G_{0.01}$ tended to be lower in the CHF rats, whereas $G_{0.1}$ and G_1 did not differ significantly between the two groups (Table 2). The phase plot showed an out-of-phase relationship in the frequency range from 0.01 to 1 Hz in both groups. The coherence plot with values less than unity suggests that SNA contained an unknown noise signal unrelated to the baroreflex and/or a nonlinear system response to the CSP input. The bottom panel of Fig. 3a represents the step responses of SNA for a unit increase in CSP. Although S_{10} and S_{50} were significantly attenuated in the CHF rats, S_{peak}, T_{peak}, and S_{peak}/S_{50} did not differ significantly between the two groups (Table 2).

The peripheral arc transfer function from SNA to AP showed low-pass characteristics (Fig. 3b). $G_{0.01}$ and $G_{0.1}$ were significantly smaller in the CHF rats, whereas G_1 did not differ significantly between the two groups (Table 2). The phase was close to zero radians at the lowest frequency and delayed with an increase in frequency in both groups. The coherence plot with values less than unity indicates that a part of AP variation was not explained by the linear dynamics with the SNA variation. In the step response of AP for a unit increase in SNA (Fig. 3b, bottom), S_{50} was significantly smaller and the initial slope (the dotted line) was significantly gentler in the CHF than in the control rats (Table 2).

The total baroreflex transfer function from CSP to AP showed low-pass characteristics (Fig. 3c). $G_{0.01}$ and $G_{0.1}$ were significantly smaller in the CHF than in the control rats (Table 2), but G_1 did not differ significantly. The phase was close to $-\pi$ radians at the lowest frequency in both groups, reflecting the negative feedback operation attained by the total baroreflex. The phase delayed with an increase in frequency. The coherence values seem lower than those in the peripheral arc transfer function. In the step response of AP for a unit increase in CSP (Fig. 3c, bottom), both S_{50} and the initial slope (the dotted line) were significantly attenuated in the CHF in comparison with the control rats (Table 2).

The transfer function from CSP to HR also displayed low-pass characteristics (Fig. 3d). $G_{0.01}$ and $G_{0.1}$ were significantly smaller in the CHF than in the control rats (Table 2). We did not compare G_1 because the coherence values close to zero and the irregular change in the phase shift above 0.8 Hz suggested poor reliability of the estimated transfer function. In the step response of HR for a unit increase in CSP (Fig. 3d, bottom), both S_{50} and the

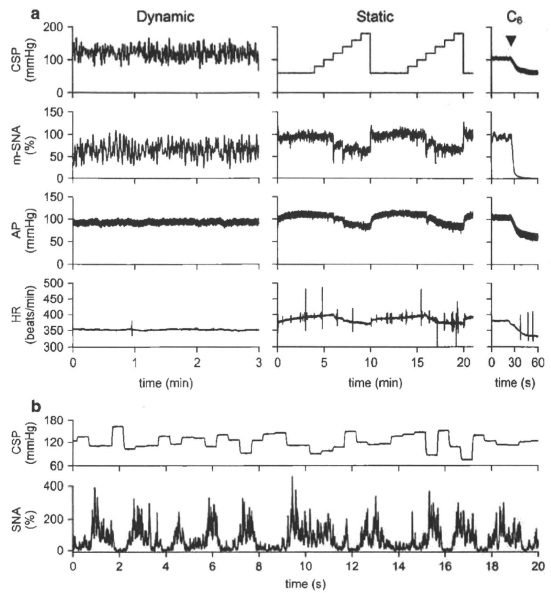

Fig. 2 **a** Typical recordings (10-Hz decimated data) of CSP, m-SNA, AP, and HR obtained from a chronic heart failure rat. In the dynamic protocol, CSP was changed according to a Gaussian white noise signal. In the static protocol, CSP was increased from 60 to 180 mmHg. The noise level of the nerve activity recorded after C_6 administration was assigned 0%, while the m-SNA value averaged for the last 10 s at CSP of 60 mmHg was assigned 100%. **b** CSP and SNA sampled at 200 Hz during the dynamic input protocol

initial slope (the dotted line) were significantly attenuated in the CHF in comparison with the control rats (Table 2).

Static characteristics of the carotid sinus baroreflex

Figure 4 summarizes the open-loop static characteristics of the carotid sinus baroreflex obtained from the control and CHF rats. The baroreflex neural arc showed a decreasing SNA response with an increase in CSP (Fig. 4a). The response range of SNA was significantly narrower in the CHF rats (Table 3). Consequently, the minimum SNA was significantly higher in the CHF rats. The midpoint pressure on the CSP axis was significantly lower in the CHF rats. Despite the significant attenuation in the response range of SNA, the maximum slope of the neural arc was not reduced in the CHF rats compared with the control rats.

The peripheral arc from SNA to AP approximated a straight line in both the control and CHF rats (Fig. 4b). The slope of the regression line was significantly less steep in the CHF rats, whereas the AP intercept did not differ significantly between the two groups (Table 3).

The total baroreflex function from CSP to AP approximated an inverse sigmoidal curve (Fig. 4c). The response range of AP was significantly narrower in the CHF rats (Table 3). The slope coefficient, the midpoint pressure on the CSP axis, and the minimum AP did not differ significantly between the two groups. The maximum gain was significantly smaller in the CHF rats compared with the control rats.

The static CSP-HR relationship also approximated an inverse sigmoidal curve (Fig. 4d). The response range of HR was significantly narrower, and the minimum HR was significantly lower in the CHF rats (Table 3). The midpoint pressure on the CSP axis was significantly lower in the CHF rats. The slope coefficient and the maximum slope did not differ significantly between the two groups.

The baroreflex equilibrium diagram is obtained by plotting the neural and peripheral arcs on a pressure-SNA plane (Fig. 4e). The ordinate is either CSP (for the neural arc) or AP (for the peripheral arc). The intersection between the neural and peripheral arcs gives the closed-loop operating point [17, 18]. The operating-point AP (the horizontal arrow) was significantly lower in the CHF rats, whereas the operating-point SNA (the vertical arrow) did not differ significantly between the two groups (Table 3). The total baroreflex gain at the operating point, calculated from the product of the tangential slope of the neural arc (ΔSNA/ΔCSP) and the slope of the peripheral arc (ΔAP/

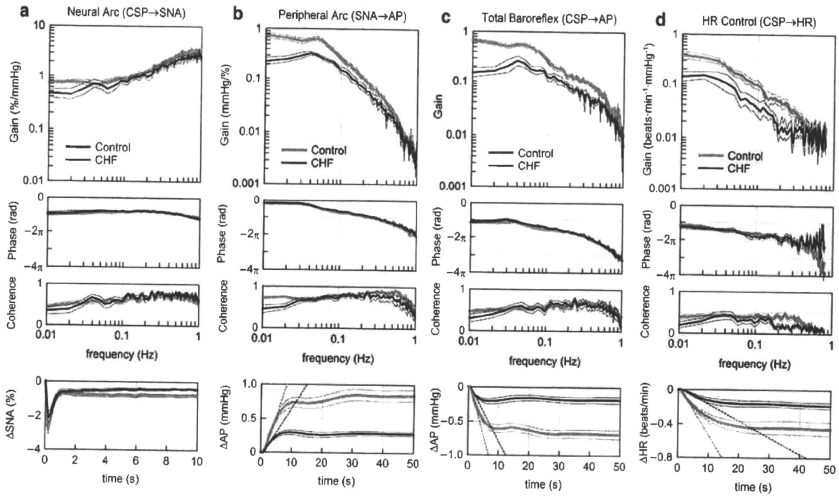

Fig. 3 Dynamic characteristics of the carotid sinus baroreflex averaged for the control rats ($n = 12$) and chronic heart failure (CHF) rats ($n = 7$). **a** Transfer function of the baroreflex neural arc from CSP to SNA. Gain, phase, and coherence plots are shown. The *bottom panel* represents the step response of SNA calculated from the transfer function. There is no significant difference in the negative peak response or the time to peak between control and CHF rats. **b** Transfer function of the baroreflex peripheral arc from SNA to AP. The *bottom panel* represents the step response of AP induced by a unit increase in SNA. Both initial slope (*dotted lines*) and steady-state response are attenuated in CHF. **c** Transfer function of the total baroreflex from CSP to AP. The *bottom panel* represents the step response of AP induced by a unit increase in CSP. Both initial slope (*dotted lines*) and steady-state response are attenuated in CHF. **d** Transfer function from CSP to HR. The *bottom panel* represents the HR step response calculated from the transfer function. Both initial slope (*dotted lines*) and steady-state response are attenuated in CHF. In each plot, *bold* and *thin lines* indicate mean and mean ± SE, respectively

ΔSNA), did not differ significantly between the two groups (Table 3): ΔCSP, ΔSNA, and ΔAP indicate small changes in CSP, SNA, and AP, respectively, at the intersection point. Figure 4f depicts a putative baroreflex equilibrium diagram where the SNA axis is scaled so that the maximum value of SNA in the CHF group becomes two times higher than that in the control group (see Discussion).

Simulation study

A block diagram of the simulation study is shown in Fig. 5a [14–16]. We used impulse responses derived from the group-averaged neural and peripheral arc transfer functions (H_N and H_P) to calculate dynamic responses of the carotid sinus baroreflex. The steady-state gains of H_N and H_P were normalized to unity in order that absolute values of the steady-state gains could be determined by their corresponding static characteristics. The static characteristics of the neural and peripheral arcs were modeled as a logistic function and a regression line, respectively, using group-averaged parameter values (Table 3). A sinusoidal wave with an amplitude of 15 mmHg (peak-to-peak pressure of 30 mmHg) and a frequency of 5 Hz (corresponding to 300 beats/min) was added to the output from the peripheral arc to mimic pulsatile pressure. The AP signal was fed back into the neural arc to achieve a closed-loop simulation. After the AP signal reached steady state, step disturbances ranging from −10 to −60 mmHg were imposed.

Typical examples of the transient AP response to a step disturbance of −40 mmHg under control and CHF conditions are shown in Fig. 5b. In each panel, the pulsatile pressure is shown in gray, and the mean AP signal is shown as a solid bold line. The horizontal dashed lines represent the mean AP values immediately before and after the onset of the step disturbance. The AP signal decreased abruptly by 40 mmHg at time zero and recovered gradually thereafter. The upward arrow indicates the magnitude of steady-state AP recovery. The recovery was greater in the control than in the CHF simulation.

Figure 5c depicts the percent recovery of AP relative to the size of the step disturbance. The steady-state AP

Table 2 Parameters of the dynamic characteristics of the carotid sinus baroreflex

	Control ($n = 12$)	CHF ($n = 7$)	P value
Neural arc			
$G_{0.01}$ (% mmHg^{-1})	0.80 ± 0.10	0.50 ± 0.08	0.051
$G_{0.1}$ (% mmHg^{-1})	0.99 ± 0.11	0.85 ± 0.14	0.432
G_1 (% mmHg^{-1})	3.49 ± 0.34	2.64 ± 0.30	0.093
S_{50} (%)	0.75 ± 0.09	0.39 ± 0.06*	0.012
S_{10} (%)	0.78 ± 0.09	0.42 ± 0.06*	0.010
S_{peak} (%)	2.88 ± 0.25	2.13 ± 0.30	0.076
T_{peak} (s)	0.29 ± 0.01	0.31 ± 0.01	0.327
S_{peak}/S_{50}	5.30 ± 1.60	6.06 ± 1.06	0.743
Peripheral arc			
$G_{0.01}$ (mmHg %$^{-1}$)	0.81 ± 0.09	0.24 ± 0.05**	<0.001
$G_{0.1}$ (mmHg %$^{-1}$)	0.29 ± 0.04	0.16 ± 0.02*	0.023
G_1 (mmHg %$^{-1}$)	0.0032 ± 0.0005	0.0050 ± 0.0015	0.211
S_{50} (mmHg)	0.84 ± 0.08	0.28 ± 0.03**	<0.001
Initial slope (mmHg s^{-1})	0.134 ± 0.014	0.071 ± 0.009**	0.007
Total baroreflex			
$G_{0.01}$ (mmHg mmHg^{-1})	0.70 ± 0.06	0.17 ± 0.03**	<0.001
$G_{0.1}$ (mmHg mmHg^{-1})	0.28 ± 0.03	0.13 ± 0.02**	0.001
G_1 (mmHg mmHg^{-1})	0.013 ± 0.002	0.010 ± 0.002	0.324
S_{50} (mmHg)	0.69 ± 0.07	0.18 ± 0.05**	<0.001
Initial slope (mmHg s^{-1})	0.166 ± 0.014	0.086 ± 0.009**	<0.001
Heart rate control			
$G_{0.01}$ (beats min^{-1} mmHg^{-1})	0.43 ± 0.06	0.16 ± 0.03**	0.005
$G_{0.1}$ (beats min^{-1} mmHg^{-1})	0.11 ± 0.02	0.04 ± 0.01*	0.026
S_{50} (beats min^{-1})	0.46 ± 0.08	0.18 ± 0.03*	0.021
Initial slope (beats min^{-1} s^{-1})	0.059 ± 0.009	0.020 ± 0.004**	0.006

Data are presented as mean ± SE

** $P < 0.01$ and * $P < 0.05$ by unpaired t test

recovery was approximately 50% in the control and approximately 32% in the CHF simulation for a step disturbance of −10 mmHg, indicating that the feedback AP regulation in the CHF simulation was approximately 64% as effective as that in the control simulation. On the other hand, the AP recovery was approximately 35% in the control and approximately 14% in the CHF simulation for a step disturbance of −60 mmHg, indicating that the efficiency of feedback AP regulation in the CHF simulation reduced to only 40% of that in the control simulation.

Figure 5d shows the initial slope of the AP recovery. The initial slope increased as the size of step disturbance increased in the control simulation. Although the initial slope of the AP recovery in the CHF simulation was comparable to that in the control simulation for a step disturbance of −10 mmHg, it did not increase significantly with an increase in the size of step disturbance.

Discussion

The major findings of the present study are (1) the dynamic characteristics of the baroreflex neural arc were preserved in CHF, whereas those of the baroreflex peripheral arc were significantly depressed (Fig. 3), and (2) the total baroreflex gain at the closed-loop operating point seemed preserved in CHF, whereas the range of baroreflex operation was significantly narrowed (Fig. 4). Because of these modulations in the baroreflex characteristics, the AP regulation was less robust against exogenous disturbances in CHF (Fig. 5), which may partly explain the incidence of acute decompensation in stable CHF patients caused by noncompliance with salt and water restriction [19].

Dynamic characteristics of the carotid sinus baroreflex in CHF rats

The derivative characteristics of the neural arc are preserved in the CHF rats (Fig. 3a), being consistent with a previous study in heart failure rabbits [20]. Moreover, the present results indicate that the dynamic AP response to SNA is significantly depressed in CHF (Fig. 3b), suggesting impaired end-organ responses to SNA. The total baroreflex function in terms of the AP regulation was more sluggish in the CHF rats (Fig. 3c, bottom) despite the preserved neural arc derivative characteristics.

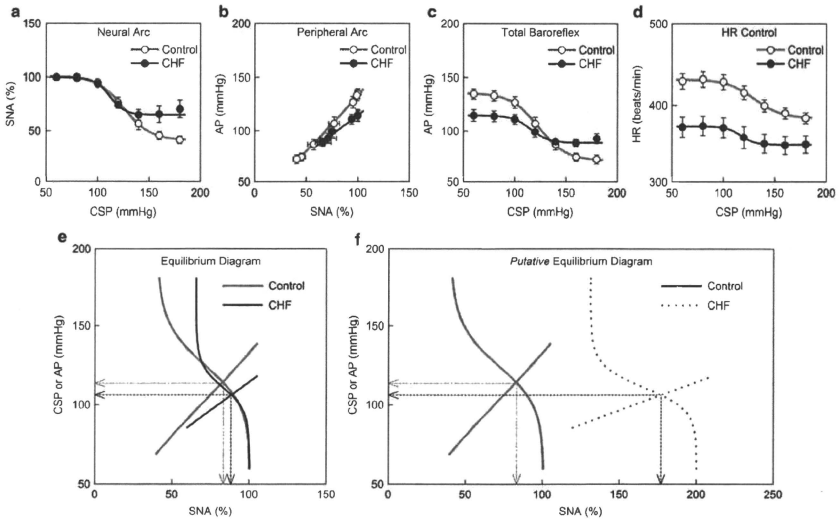

Fig. 4 Static characteristics of the carotid sinus baroreflex averaged for the control ($n = 12$) and chronic heart failure (CHF; $n = 7$) rats. **a** Static characteristics of the baroreflex neural arc. An increase in CSP decreases SNA. The response range in SNA is significantly attenuated in CHF. **b** Static characteristics of the baroreflex peripheral arc. An increase in SNA increases AP in a linear manner. The slope of the regression line is significantly gentler in CHF. **c** Static characteristics of the total baroreflex. CSP and AP show an inverse sigmoidal relationship. The response range of AP and the maximum gain are significantly smaller in CHF. **d** Static characteristics between CSP and HR. CSP and HR show an inverse sigmoidal relationship. The response range of HR and the minimum HR are significantly smaller in CHF. **e** Baroreflex equilibrium diagram constructed from the fitted logistic function for the neural arc and the regression line for the peripheral arc. **f** Putative baroreflex equilibrium diagram in which the SNA axis is scaled so that the maximum absolute SNA in CHF becomes two times higher than that in control. In panels **e** and **f**, the *dotted lines* with *arrowheads* indicate the operating-point AP and SNA in CHF. The *dash-dot lines* with *arrowheads* indicate the operating-point AP and SNA in control

In the transfer function from CSP to HR, dynamic gain values were significantly attenuated in the CHF rats (Fig. 3d). Because the dynamic gain of the neural arc transfer function did not reduce significantly ($G_{0.1}$), the attenuation of the dynamic gain of the HR control may be attributable to the reduced HR response to SNA such as that related to the downregulation of β-adrenergic receptors [21].

Static characteristics of the carotid sinus baroreflex in CHF rats

In both the control and CHF rats, the input-output relationship of the peripheral arc approximated a straight line (Fig. 4b), and the sigmoidal nonlinearity is primarily attributed to the neural arc (Fig. 4a). The impairment of the total baroreflex in the CHF rats, characterized by a significant attenuation of the response range of AP and a reduction of the maximum gain (Fig. 4c, Table 3), is in essence similar to that obtained previously in canine models of heart failure [3, 5, 6].

Wang et al. [4, 5] reported poor end-organ responses and normal central control of renal SNA in the heart failure dogs. The attenuated slope of the peripheral arc in the CHF rats (Fig. 4b) may be consistent with the poor end-organ responses. Although the response range of SNA in the neural arc was narrowed in the CHF rats (Fig. 4a), the maximum slope of the neural arc did not change significantly, which should contribute to the maintained total baroreflex gain within a small range around the operating point (Fig. 4e, Table 3).

The response range of HR was significantly reduced in the CHF rats (Fig. 4d) in agreement with the depressed dynamic HR response to CSP (Fig. 3d). Although 24-h averaged HR was higher in the CHF rats in a previous study [7], the minimum HR was significantly lower in the CHF than in the control rats. Anesthesia and vagotomy might have affected the results, and further studies are

Table 3 Parameters of the static characteristics of the carotid sinus baroreflex

	Control ($n = 12$)	CHF ($n = 7$)	P value
Neural arc			
P_1, response range (%)	62 ± 4	42 ± 6**	0.008
P_2, slope coefficient ($mmHg^{-1}$)	0.10 ± 0.01	0.16 ± 0.03*	0.048
P_3, midpoint pressure (mmHg)	128 ± 4	115 ± 4*	0.043
P_4, minimum SNA (%)	39 ± 4	60 ± 6**	0.008
Maximum slope (% $mmHg^{-1}$)	1.62 ± 0.27	1.54 ± 0.27	0.839
Peripheral arc			
a, slope (mmHg $\%^{-1}$)	1.10 ± 0.08	0.75 ± 0.10*	0.013
b, AP intercept (mmHg)	23.5 ± 7.7	40.7 ± 7.2	0.152
Total baroreflex			
P_1, response range (mmHg)	64 ± 4	31 ± 6**	<0.001
P_2, slope coefficient ($mmHg^{-1}$)	0.10 ± 0.01	0.13 ± 0.01	0.144
P_3, midpoint pressure (mmHg)	122 ± 3	117 ± 4	0.326
P_4, minimum AP (mmHg)	74 ± 4	85 ± 3	0.065
Maximum gain	1.62 ± 0.22	0.95 ± 0.17*	0.048
Heart rate control			
P_1, response range (beats min^{-1})	49 ± 5	30 ± 6*	0.033
P_2, slope coefficient ($mmHg^{-1}$)	0.10 ± 0.01	0.13 ± 0.01	0.099
P_3, midpoint pressure (mmHg)	131 ± 4	117 ± 4*	0.046
P_4, minimum HR (beats min^{-1})	383 ± 7	343 ± 13*	0.011
Maximum slope (beats min^{-1} $mmHg^{-1}$)	1.28 ± 0.23	0.93 ± 0.20	0.313
Equilibrium diagram			
Operating-point AP (mmHg)	116 ± 3	106 ± 3*	0.042
Operating-point SNA (%)	84 ± 3	90 ± 4	0.227
Operating-point total baroreflex gain	1.23 ± 0.28	0.96 ± 0.39	0.578

Data are presented as mean ± SE

** $P < 0.01$ and * $P < 0.05$ by unpaired t test

needed to reconcile some of the discrepancies between the present and previous results.

Equilibrium diagram and simulation study

A baroreflex equilibrium diagram provides information on the closed-loop operating point (Fig. 4e) [10, 17, 18, 22–26]. Because absolute SNA is considered to be higher in CHF [7], if we can use the absolute value for SNA, the SNA axis of the equilibrium diagram should be scaled in a manner that renders the peripheral arc much shallower in the CHF than in the control rats (Fig. 4f). The operating-point AP was decreased only by 10 mmHg in the CHF rats and the total baroreflex gain at the operating point did not differ between the control and CHF rats. The baroreflex function may therefore seem preserved in the CHF rats when it is assessed only within a small range around the closed-loop operating point.

We used splanchnic SNA to construct a baroreflex equilibrium diagram. The analysis based on SNA of only one limb of the sympathetic nervous system can be an oversimplification in light of the well-known regional differences in SNAs [27–29]. One rationale for using splanchnic SNA is that the splanchnic region has been regarded as a major site for the blood flow redistribution [17, 30]. Furthermore, we have continued to observe insignificant differences in the steady-state responses to CSP between left and right cardiac SNAs [31], between cardiac and renal SNAs [32], and among cardiac, renal, and muscle SNAs [33] in anesthetized rabbits. It seems that the carotid sinus baroreflex brings about common activity in addition to regional activity among sympathetic nerves innervating several districts (see Appendix 3). Whether the similarity among SNAs to different districts will hold in other experimental conditions awaits future investigations.

The simulation study is useful and necessary for the integrated understanding of the estimated dynamic and static characteristics of the carotid sinus baroreflex (Fig. 5a). The feedback AP regulation becomes much weaker in CHF as the size of step disturbance increases (Fig. 5c, d), suggesting that a reserve for AP buffering is lost in CHF. Because not only the baroreceptor input but also loading conditions to the heart are changed during orthostatic tilt, the results of the present simulation can not be directly extrapolated to the actual tilting conditions. However, it may be of notice that patients with severe congestive heart failure show a significant drop in systolic AP upon orthostatic tilt regardless of relatively maintained

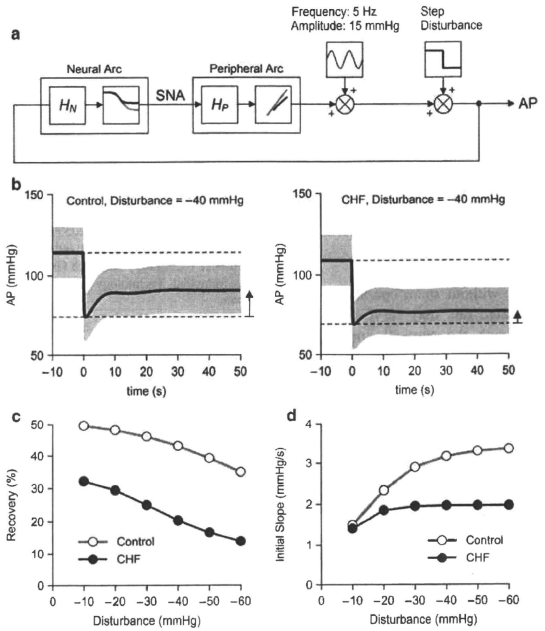

Fig. 5 **a** Block diagram for the simulation of AP regulation. H_N and H_P represent dynamic characteristics of the neural and peripheral arcs, respectively. The static characteristics of the neural arc were modeled as a logistic function. The static characteristics of the peripheral arc were modeled as a straight line. Parameters for the logistic function and the regression line were derived from mean values shown in Table 3. A 5-Hz sine wave with an amplitude of 15 mmHg was added to mimic pulsatile pressure. Exogenous step disturbances ranging from −10 to −60 mmHg were applied, and the closed-loop AP responses were calculated for control and CHF conditions. **b** Typical simulation results during an exogenous pressure disturbance of −40 mmHg. The pulsatile pressure is shown in *gray*, and mean AP signal is shown as a *bold line*. The *horizontal dotted lines* indicate the mean AP values just before and after the onset of step disturbance. AP recovers less efficiently in the CHF simulation compared to the control simulation. **c** Percent recovery of AP as a function of the size of disturbance. **d** The initial slope of the recovery as a function of the size of disturbance

baseline AP [34]. The exogenous disturbance in the opposite direction may also be hazardous. Even though baseline AP appears normal in stable CHF patients, non-compliance with salt and water restriction may easily collapse the AP regulation and induce acute decompensation [19].

Study perspective

The progression of CHF is closely associated with the autonomic imbalance between sympathetic and vagal nerve activities. Although pharmacological treatments such as β-adrenergic blockers [35], angiotensin converting enzyme inhibitors [36], and angiotensin receptor blockers [37] have been developed, the therapeutic outcome is not always satisfactory and the mortality rate for CHF remains high. Novel therapeutic strategies for CHF beyond conventional treatments such as electrical vagal nerve stimulation are expected to be developed [7, 38].

Although the mechanisms for the autonomic imbalance in CHF are not completely understood, the loss of baroreflex control of the sympathetic and vagal systems has been considered an important factor [39, 40]. Zucker et al. [41] demonstrated that chronic baroreceptor activation improved the survival of dogs with pacing-induced heart failure. The study seems rudimentary, however, in that the stimulation intensity of the carotid sinus baroreceptors was adjusted intermittently to obtain a prescribed sympathoinhibitory response. The stimulation could be too strong or too weak during the intervals of adjustments. If the

stimulation intensity is feedback-controlled continuously, the therapeutic effect and safety could be enhanced.

Quantification of the dynamic characteristics of a target system is the first step for developing a robust controller [42–44]. Next, the controller should be designed in such a way that the variation of the target system dynamics does not affect the controlling result much [45]. The simulation of the closed-loop AP response in CHF, such as that shown in Fig. 5, will be utilized in designing a robust controller system of the carotid sinus activation.

Limitations

First, we used normal rats without sham operation as the control group. Sham-operated rats may serve as a more appropriate control. Although the surgical operation of thoracotomy itself could have affected the baroreflex function in the CHF group, because over 100 days had elapsed after the surgical operation, the effect of surgical operation might have been limited. Actually, two rats that underwent coronary ligation but did not meet the criteria for CHF retained the maximum gain of the total baroreflex close to the control group (rat A: central venous pressure = 2.28 mmHg, biventricular weight = 1.94 g kg^{-1}, total baroreflex gain = 1.61; rat B: central venous pressure = 1.69 mmHg, biventricular weight = 2.33 g kg^{-1}, total baroreflex gain = 1.67).

Second, the data were obtained under anesthetic conditions. Because the anesthesia affects autonomic nervous activities, the results should be carefully interpreted. Vagotomy and lower perfusion of the brain due to carotid artery occlusion might have also affected the baroreflex function. Nevertheless, the present results would provide a unique clue to integrated understanding of the impaired baroreflex function in CHF.

Third, we did not measure cardiac output or peripheral vascular resistance. Subdividing the peripheral arc into the cardiac and vascular components will be necessary to identify the mechanisms for an approximately linear relationship between SNA and AP in both the control and CHF rats.

Conclusions

The dynamic and static characteristics of the neural arc, peripheral arc, and total baroreflex were analyzed comprehensively in rats with CHF after myocardial infarction. Although the derivative characteristics of the baroreflex neural arc are preserved in the CHF rats, the dynamic AP regulation is depressed in both the magnitude and response speed. The equilibrium diagram indicates that the baroreflex gain may seem preserved in CHF in a small range around the closed-loop operating point. However, the percent recovery of AP and the speed of recovery are reduced progressively as the size of exogenous disturbance increases in the CHF rats. The reserve for AP buffering may be lost in CHF despite the relatively maintained baseline AP.

Acknowledgments This study was supported by Health and Labour Sciences Research Grants (H18-nano-Ippan-003, H19-nano-Ippan-009, H20-katsudo-Shitei-007, and H21-nano-Ippan-005) from the Ministry of Health, Labour and Welfare of Japan; by a Grant-in-Aid for Scientific Research (No. 20390462) from the Ministry of Education, Culture, Sports, Science and Technology of Japan; and by the Industrial Technology Research Grant Program from the New Energy and Industrial Technology Development Organization (NEDO) of Japan.

Appendix 1: feature of a Gaussian white noise input

The neural arc of the arterial baroreflex may be roughly modeled by a cascade system, which consists of a dynamic linear subsystem followed by a static nonlinear subsystem [14]. In this type of system, the selection of the mean input pressure and the amplitude of input does not significantly affect the estimation of the system linear dynamics except for a factor of proportionality when the system is tested with a Gaussian white noise (GWN) signal [46]. In order to demonstrate the above notion, we performed a simulation study. In reference to Fig. 6a, the dynamic linear subsystem for the baroreflex neural arc was modeled by the following equation:

$$H_N(f) = \frac{1 + \frac{f}{f_{C1}}j}{\left(1 + \frac{f}{f_{C2}}j\right)^2}\exp(-2\pi fjL) \tag{5}$$

where f_{C1} and f_{C2} are the corner frequencies determining the frequency-dependent changes in the dynamic gain, L denotes the pure dead time, f and j indicate frequency and an imaginary unit, respectively. We set $f_{C1} = 0.1$ Hz, $f_{C2} = 0.9$ Hz, and $L = 0.1$ s to mimic the neural arc transfer function. The static nonlinear subsystem of the neural arc was modeled by the logistic function (Eq. 3) with parameters of $P_1 = 60\%$, $P_2 = 0.1$ $mmHg^{-1}$, $P_3 = 120$ mmHg, and $P_4 = 40\%$. Using this model, the linear input-output relationship was estimated by a GWN input or a binary white noise (BIN) input. Mean input pressure was changed among 120, 90, and 150 mmHg (P_3, $P_3 - 30$, and $P_3 + 30$ mmHg).

Figure 6b through 6d shows the estimation results. In each panel, thin smooth curves in the gain and phase plots indicate the transfer function of the dynamic linear subsystem described by Eq. 5. The solid bold curves, dotted thin curves, and dashed thin curves represent the estimation

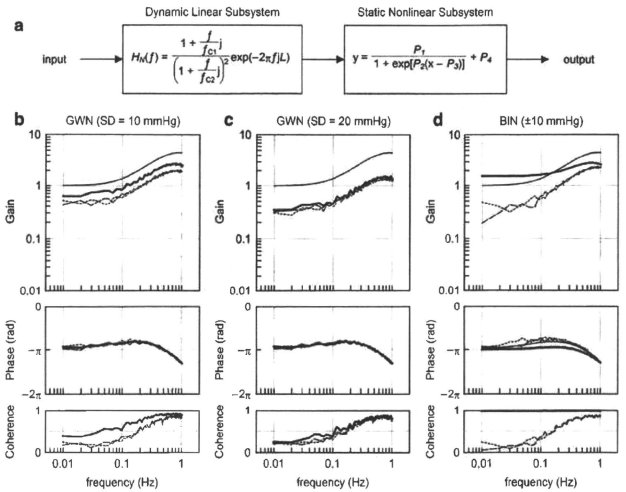

Fig. 6 **a** A cascade model for the baroreflex neural arc, which consists of a dynamic linear subsystem and a static nonlinear subsystem. The dynamic linear subsystem represents the neural arc transfer function. The static nonlinear subsystem represents the sigmoidal nonlinearity for the neural arc. **b** Estimation results of the system dynamic characteristics using a Gaussian white noise (GWN) input with a standard deviation (SD) of 10 mmHg. **c** Estimation results of the system dynamic characteristics using a GWN input with an SD of 20 mmHg. **d** Estimation results of the system dynamic characteristics using a binary white noise (BIN) input with an amplitude of 10 mmHg. In panels **b** through **d**, the *thin smooth curve* indicates the transfer function of the given dynamic linear subsystem. The *solid bold curve*, *dotted thin curve*, and *dashed thin curve* represent the estimation results obtained by the input signals with mean input pressures of 120, 90, and 150 mmHg, respectively (see text for explanation)

results obtained by mean input pressures of 120, 90, and 150 mmHg, respectively. Figure 6b and c represents the estimation results obtained by GWNs with standard deviations of 10 and 20 mmHg, respectively. As can be seen, the estimated gain plots are nearly parallel to the gain plot of the given dynamic linear subsystem. The estimated phase plots are superimposable on the phase plot of the given dynamic linear subsystem.

Figure 6d shows the estimation results obtained by BINs with an amplitude of 10 mmHg (i.e., the peak-to-peak pressure of 20 mmHg). None of the estimated gain plots are parallel to the gain plot of the given dynamic linear subsystem. The estimated phase plots also deviated from the phase plot of the given dynamic linear subsystem. When the system was tested by the BIN input with the mean input pressure of 120 mmHg, the coherence value became close to unity, suggesting that the BIN input had caused on-off behavior in the system output.

The above simulation results confirm that the selection of the mean input pressure and the amplitude of GWN does not significantly affect the estimation of the dynamic characteristics of the system except for a factor of proportionality when the mean input pressure and the standard deviation of GWN are not far beyond the system operating range.

Appendix 2: estimation of the initial slope of the step response or recovery response

To characterize the speed of the response, the initial slope of the response was calculated as follows. First, a response threshold is determined as the 5% value of the steady-state step response. In the case of the recovery response, 5% of the maximum recovery is used as the threshold. Next, an initial time point at which the response exceeds the threshold value is determined. Starting from this initial time point, a linear regression analysis giving a slope and an intercept is performed repeatedly while increasing the number of analyzed data points. The steepest slope thus

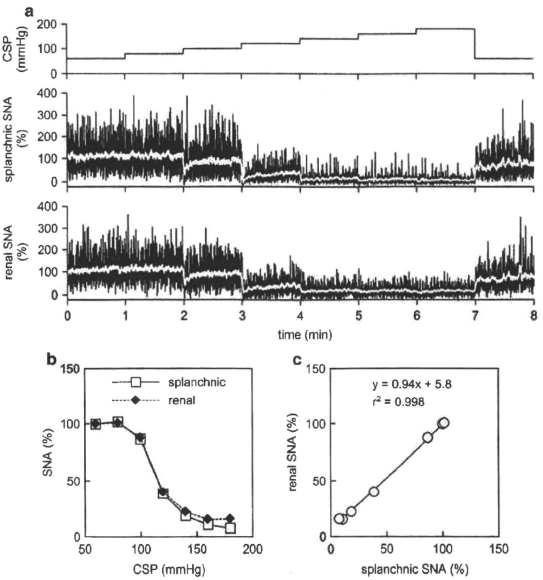

Fig. 7 **a** Typical recordings of 10-Hz decimated CSP, splanchnic SNA, and renal SNA obtained from a normal rat in an additional study using the same experimental settings as the main study. The *white lines* in the SNA recordings represent 2-s moving averaged signals. An increase in CSP decreased splanchnic and renal SNAs. **b** Static characteristics of the baroreflex neural arc drawn based on splanchnic and renal SNAs. **c** Correlation between splanchnic and renal SNAs during the stepwise input protocol. In panels **b** and **c**, splanchnic and renal SNA data were obtained as the averaged values during the last 10 s at each CSP level

obtained is used as the initial slope of the response. By setting the 5% threshold, the linear regression can be performed excluding the initial data points constituting the dead time.

Appendix 3: comparison of splanchnic and renal SNAs under the present experimental conditions

We compared splanchnic and renal SNAs under the present experimental conditions in an additional three rats. A branch of the right renal sympathetic nerve was exposed through a right flank incision, and renal SNA was recorded simultaneously with splanchnic SNA. Figure 7a presents time series of 10-Hz decimated CSP, splanchnic SNA, and renal SNA obtained from one rat. White lines in splanchnic and renal SNAs indicate 2-s moving averaged signals. In each of the splanchnic and renal SNAs, a 10-s averaged value for the last 10 s at CSP of 60 mmHg was defined as 100%, and a 10-s averaged value after the administration of hexamethonium bromide was defined as 0%, in the same manner as the main study. Figure 7b shows the relationships of SNAs versus CSP. Although the renal SNA values were slightly greater than the splanchnic SNA values at CSPs of 160 and 180 mmHg in this rat, the general sigmoidal relationships were similar between the two SNAs. The regression line for renal SNA (y) versus splanchnic SNA (x) was $y = 0.94x + 5.8$ ($r^2 = 0.998$) in this rat (Fig. 7c). The other two rats showed regression lines of $y = 1.01x + 0.3$ ($r^2 = 0.999$) and $y = 0.99x + 3.7$ ($r^2 = 0.995$), suggesting that both splanchnic and renal SNAs can represent common activity for the AP regulation during the stepwise input protocol under the present experimental conditions.

References

1. Ikeda Y, Kawada T, Sugimachi M, Kawaguchi O, Shishido T, Sato T, Miyano H, Matsuura W, Alexander J Jr, Sunagawa K (1996) Neural arc of baroreflex optimizes dynamic pressure regulation in achieving both stability and quickness. Am J Physiol 271:H882–H890
2. Sato T, Kawada T, Inagaki M, Shishido T, Sugimachi M, Sunagawa K (2003) Dynamics of sympathetic baroreflex control of arterial pressure in rats. Am J Physiol Regul Integr Comp Physiol 285:R262–R270
3. White CW (1981) Abnormalities in baroreflex control of heart rate in canine heart failure. Am J Physiol 240:H793–H799
4. Wang W, Chen JS, Zucker IH (1990) Carotid sinus baroreceptor sensitivity in experimental heart failure. Circulation 81:1959–1966

5. Wang W, Chen JS, Zucker IH (1991) Carotid sinus baroreceptor reflex in dogs with experimental heart failure. Circ Res 68:1294–1301
6. Wang W, Brändle M, Zucker IH (1993) Influence of vagotomy on the baroreflex sensitivity in anesthetized dogs with experimental heart failure. Am J Physiol 265:H1310–H1317
7. Li M, Zheng C, Sato T, Kawada T, Sugimachi M, Sunagawa K (2004) Vagal nerve stimulation markedly improves long-term survival after chronic heart failure in rats. Circulation 109:120–124
8. Shoukas AA, Callahan CA, Lash JM, Haase EB (1991) New technique to completely isolate carotid sinus baroreceptor regions in rats. Am J Physiol 260:H300–H303
9. Sato T, Kawada T, Miyano H, Shishido T, Inagaki M, Yoshimura R, Tatewaki T, Sugimachi M, Alexander J Jr, Sunagawa K (1999) New simple methods for isolating baroreceptor regions of carotid sinus and aortic depressor nerves in rats. Am J Physiol 276:H326–H332
10. Kawada T, Kamiya A, Li M, Shimizu S, Uemura K, Yamamoto H, Sugimachi M (2009) High levels of circulating angiotensin II shift the open-loop baroreflex control of splanchnic sympathetic nerve activity, heart rate and arterial pressure in anesthetized rats. J Physiol Sci 59:447–455
11. Marmarelis PZ, Marmarelis VZ (1978) The white noise method in system identification. In: Analysis of physiological systems. Plenum, New York, pp 131–221
12. Kent BB, Drane JW, Blumenstein B, Manning JW (1972) A mathematical model to assess changes in the baroreceptor reflex. Cardiology 57:295–310
13. Glantz SA (2002) Primer of biostatistics, 5th edn. McGraw-Hill, New York
14. Kawada T, Yanagiya Y, Uemura K, Miyamoto T, Zheng C, Li M, Sugimachi M, Sunagawa K (2003) Input-size dependence of the baroreflex neural arc transfer characteristics. Am J Physiol Heart Circ Physiol 284:H404–H415
15. Yamamoto K, Kawada T, Kamiya A, Takaki H, Shishido T, Sunagawa K, Sugimachi M (2008) Muscle mechanoreflex augments arterial baroreflex-mediated dynamic sympathetic response to carotid sinus pressure. Am J Physiol Heart Circ Physiol 295:H1081–H1089
16. Kamiya A, Kawada T, Yamamoto K, Mizuno M, Shimizu S, Sugimachi M (2008) Upright tilt resets dynamic transfer function of baroreflex neural arc to minify the pressure disturbance in total baroreflex control. J Physiol Sci 58:189–198
17. Mohrman DE, Heller LJ (2006) Cardiovascular physiology, 6th edn. McGraw Hill, New York
18. Sato T, Kawada T, Inagaki M, Shishido T, Takaki H, Sugimachi M, Sunagawa K (1999) New analytic framework for understanding sympathetic baroreflex control of arterial pressure. Am J Physiol 276:H2251–H2261
19. Lepage S (2008) Acute decompensated heart failure. Can J Cardiol 24(Suppl B):6B–8B
20. Masaki H, Imaizumi T, Harasawa Y, Takeshita A (1994) Dynamic arterial baroreflex in rabbits with heart failure induced by rapid pacing. Am J Physiol 267:H92–H99
21. Kawai H, Mohan A, Hagen J, Dong E, Armstrong J, Stevens SY, Liang CS (2000) Alterations in cardiac adrenergic terminal function and β-adrenoceptor density in pacing-induced heart failure. Am J Physiol Heart Circ Physiol 278:H1708–H1716
22. Kawada T, Shishido T, Inagaki M, Zheng C, Yanagiya Y, Uemura K, Sugimachi M, Sunagawa K (2002) Estimation of baroreflex gain using a baroreflex equilibrium diagram. Jpn J Physiol 52:21–29
23. Kashihara K, Kawada T, Li M, Sugimachi M, Sunagawa K (2004) Bezold-Jarisch reflex blunts arterial baroreflex via the shift of neural arc toward lower sympathetic nerve activity. Jpn J Physiol 54:395–404
24. Yamamoto K, Kawada T, Kamiya A, Takaki H, Miyamoto T, Sugimachi M, Sunagawa K (2004) Muscle mechanoreflex induces the pressor response by resetting the arterial baroreflex neural arc. Am J Physiol Heart Circ Physiol 286:H1382–H1388
25. Kamiya A, Kawada T, Yamamoto K, Michikami D, Ariumi H, Uemura K, Zheng C, Shimizu S, Aiba T, Miyamoto T, Sugimachi M, Sunagawa K (2005) Resetting of the arterial baroreflex increases orthostatic sympathetic activation and prevents postural hypotension in rabbits. J Physiol 566:237–246
26. Michikami D, Kamiya A, Kawada T, Inagaki M, Shishido T, Yamamoto K, Ariumi H, Iwase S, Sugenoya J, Sunagawa K, Sugimachi M (2006) Short-term electroacupuncture at Zusanli resets the arterial baroreflex neural arc toward lower sympathetic nerve activity. Am J Physiol Heart Circ Physiol 291:H318–H326
27. Ninomiya I, Nisimaru N, Irisawa H (1971) Sympathetic nerve activity to the spleen, kidney, and heart in response to baroceptor input. Am J Physiol 221:1346–1351
28. Matsukawa K, Ninomiya I, Nishiura N (1993) Effects of anesthesia on cardiac and renal sympathetic nerve activities and plasma catecholamines. Am J Physiol 265:R792–R797
29. Yamamoto H, Kawada T, Kamiya A, Kita T, Sugimachi M (2008) Electroacupuncture changes the relationship between cardiac and renal sympathetic nerve activities in anesthetized cats. Auton Neurosci 144:43–49
30. Rowell LB (1974) Human cardiovascular adjustments to exercise and thermal stress. Physiol Rev 54:75–159
31. Kawada T, Uemura K, Kashihara K, Jin Y, Li M, Zheng C, Sugimachi M, Sunagawa K (2003) Uniformity in dynamic baroreflex regulation of left and right cardiac sympathetic nerve activities. Am J Physiol Regul Integr Comp Physiol 284:R1506–R1512
32. Kawada T, Shishido T, Inagaki M, Tatewaki T, Zheng C, Yanagiya Y, Sugimachi M, Sunagawa K (2001) Differential dynamic baroreflex regulation of cardiac and renal sympathetic nerve activities. Am J Physiol Heart Circ Physiol 280:H1581–H1590
33. Kamiya A, Kawada T, Yamamoto K, Michikami D, Ariumi H, Miyamoto T, Shimizu S, Uemura K, Aiba T, Sunagawa K, Sugimachi M (2005) Dynamic and static baroreflex control of muscle sympathetic nerve activity (SNA) parallels that of renal and cardiac SNA during physiological change in pressure. Am J Physiol Heart Circ Physiol 289:H2641–H2648
34. Kassis E (1987) Cardiovascular response to orthostatic tilt in patients with severe congestive heart failure. Cardiovasc Res 21:362–368
35. Packer M, Fowler MB, Roecker EB, Coats AJ, Katus HA, Krum H, Mohacsi P, Rouleau JL, Tendera M, Staiger C, Holcslaw TL, Amann-Zalan I, DeMets DL (2002) Effect of carvedilol on the morbidity of patients with severe chronic heart failure: results of the Carvedilol Prospective Randomized Cumulative Survival (COPERNICUS) study. Circulation 106:2194–2199
36. Yusuf S, Sleight P, Pogue J, Bosch J, Davies R, Dagenais G (2000) Effects of an angiotensin-converting-enzyme inhibitor, ramipril, on cardiovascular events in high-risk patients. The heart outcomes prevention evaluation study investigators. N Engl J Med 342:145–153
37. Telmisartan Randomised AssessmeNt Study in ACE iNtolerant subjects with cardiovascular Disease (TRANSCEND) Investigators, Yusuf S, Teo K, Anderson C, Pogue J, Dyal L, Copland I, Schumacher H, Dagenais G, Sleight P (2008) Effects of the angiotensin-receptor blocker telmisartan on cardiovascular events in high-risk patients intolerant to angiotensin-converting enzyme inhibitors: a randomised controlled trial. Lancet 372:1174–1183

38. Schwartz PJ, De Ferrari GM, Sanzo A, Landolina M, Rordorf R, Raineri C, Campana C, Revera M, Ajmone-Marsan N, Tavazzi L, Odero A (2008) Long term vagal stimulation in patients with advanced heart failure: first experience in man. Eur J Heart Fail 10:884–891
39. Mancia G, Seravalle G, Giannattasio C, Bossi M, Preti L, Cattaneo BM, Grassi G (1992) Reflex cardiovascular control in congestive heart failure. Am J Cardiol 69:17G–23G
40. Eckberg DL, Drabinsky M, Braunwald E (1971) Defective cardiac parasympathetic control in patients with heart disease. N Engl J Med 285:877–883
41. Zucker IH, Hackley JF, Cornish KG, Hiser BA, Anderson NR, Kieval R, Irwin ED, Serdar DJ, Peuler JD, Rossing MA (2007) Chronic baroreceptor activation enhances survival in dogs with pacing-induced heart failure. Hypertension 50:904–910
42. Sato T, Kawada T, Sugimachi M, Sunagawa K (2002) Bionic technology revitalizes native baroreflex function in rats with baroreflex failure. Circulation 106:730–734
43. Gotoh TM, Tanaka K, Morita H (2005) Controlling arterial blood pressure using a computer-brain interface. Neuroreport 16:343–347
44. Kawada T, Shimizu S, Yamamoto H, Shishido T, Kamiya A, Miyamoto T, Sunagawa K, Sugimachi M (2009) Servo-controlled hind-limb electrical stimulation for short-term arterial pressure control. Circ J 73:851–859
45. Åström K, Hägglund T (1995) PID controllers: theory, design, and tuning, 2nd edn. International Society of Automation, Research Triangle Park, NC
46. Hunter IW, Korenberg MJ (1986) The identification of nonlinear biological systems: Wiener and Hammerstein cascade models. Biol Cybern 55:135–144

Autonomic Neuroscience: Basic and Clinical 156 (2010) 149–151

Contents lists available at ScienceDirect

Autonomic Neuroscience: Basic and Clinical

journal homepage: www.elsevier.com/locate/autneu

Short communication

Large conductance Ca^{2+}-activated K^+ channels inhibit vagal acetylcholine release at the rabbit sinoatrial node

Toru Kawada [a,*], Tsuyoshi Akiyama [b], Shuji Shimizu [a], Atsunori Kamiya [a], Kazunori Uemura [a], Yusuke Sata [a], Mikiyasu Shirai [b], Masaru Sugimachi [a]

[a] Department of Cardiovascular Dynamics, National Cerebral and Cardiovascular Center Research Institute, Osaka, Japan
[b] Department of Cardiac Physiology, National Cerebral and Cardiovascular Center Research Institute, Osaka, Japan

ARTICLE INFO

Article history:
Received 15 January 2010
Received in revised form 1 April 2010
Accepted 9 April 2010

Keywords:
Acetylcholine
Cardiac microdialysis
Vagal stimulation
Rabbits

ABSTRACT

Although large conductance Ca^{2+}-activated K^+ (BK) channels play an important role in determining vascular tone, their role in the efferent cardiac vagal system remains to be elucidated. In anesthetized rabbits ($n=9$), acetylcholine (ACh) was measured at the right atrium near the sinoatrial node by a cardiac microdialysis technique, and the ACh release in response to electrical stimulation of the cervical preganglionic vagal nerves was examined. Local administration of a BK channel blocker iberiotoxin (2 μM) through a dialysis fiber increased the stimulation-induced ACh release from 7.6 ± 2.7 to 9.0 ± 3.2 nM ($P<0.05$). Addition of intravenous administration of iberiotoxin (0.11 mg/body) did not increase the stimulation-induced ACh release further (10.8 ± 4.4 nM). These results indicate that the BK channels play an inhibitory role in the vagal ACh release to the sinoatrial node.

1. Introduction

Ca^{2+}-activated K^+ channels are located in the vicinity of voltage-dependent Ca^{2+} channels. Their activation induces outward efflux of K^+, leading to hyperpolarization of the plasma membrane and promoting closure of the voltage-dependent Ca^{2-} channels. Among the group of Ca^{2+}-activated K^+ channels, large conductance Ca^{2+}-activated K^+ channels, also designated as the "Big K" (BK) channels, are expressed in the plasma membrane of vascular smooth muscle cells and contribute to the regulation of vascular tone (Ledoux et al., 2006). The BK channels are also found on neural cells and play a critical role in shaping action potentials and modifying firing patterns (Pedarzani et al., 2000). Blockade of the BK channels by iberiotoxin enhanced presynaptic release of acetylcholine (ACh) and postsynaptic release of catecholamine in the rat adrenal medulla during electrical stimulation of the splanchnic nerve, suggesting an inhibitory role of the BK channels in the physiological catecholamine release from the adrenal medulla (Akiyama et al., 2010). The role of the BK channels in the efferent vagal system in controlling the heart, however, remains to be elucidated. If the BK channels limit Ca^{2+} entry through the voltage-dependent Ca^{2+} channels in the preganglionic and/or postganglionic vagal nerve terminals, blockade of the BK channels by iberiotoxin would enhance the ACh release in response to electrical stimulation of the preganglionic vagal nerve. A recent development of a cardiac microdialysis technique in the in vivo rabbit right atrium has enabled direct monitoring of vagal ACh release to the sinoatrial node (Shimizu et al., 2009). This technique was used to examine the role of the BK channels in the efferent cardiac vagal system.

2. Materials and methods

Animal care was conducted in accordance with the *Guiding Principles for the Care and Use of Animals in the Field of Physiological Sciences*, which has been approved by the Physiological Society of Japan. All experimental protocols were reviewed and approved by the Animal Subjects Committee at the National Cerebral and Cardiovascular Center. Nine Japanese white rabbits weighing 2.3 kg to 3.0 kg were anesthetized via intravenous administration of pentobarbital sodium (30–35 mg/kg) through a marginal ear vein. A tracheal tube was inserted through a midline cervical incision. The animal was ventilated mechanically with room air mixed with oxygen through the tracheal tube. The anesthesia was maintained using a continuous intravenous infusion of urethane (125 mg/kg h^{-1}) and α-chloralose (20 mg/kg h^{-1}) through a catheter inserted into the right femoral vein. Mean arterial pressure (AP) was measured by a biological amplifier unit 2238 (San-ei, Japan) using a fluid-filled transducer (BD DTXPlus, Becton, Dickinson and Company) connected to a catheter inserted into the right femoral artery. Heart rate (HR) was derived from an electrocardiogram. Through a midline thoracotomy, the right thymus was removed. A main branch of the right cardiac sympathetic nerve was sectioned to reduce a possible

* Corresponding author. Department of Cardiovascular Dynamics, National Cerebral and Cardiovascular Center Research Institute, 5-7-1 Fujishirodai, Suita, Osaka 565-8565, Japan. Tel.: +81 6 6833 5012 x 2427; fax: +81 6 6835 5403.
E-mail address: torukawa@res.ncvc.go.jp (T. Kawada).

1566-0702/$ – see front matter © 2010 Elsevier B.V. All rights reserved.
doi:10.1016/j.autneu.2010.04.003

sympatho-vagal interaction in the ACh release. After incising the pericardium, a dialysis probe was implanted within the right atrial wall near the junction with the superior vena cava where the sinoatrial node resides (Shimizu et al., 2009). Bilateral vagal nerves were exposed and sectioned at the neck. A pair of platinum electrodes was attached to each sectioned nerve to stimulate the efferent vagal nerve. The dialysis probe was examined postmortem to confirm that it did not penetrate into the atrial cavity.

Acetylcholine was measured in the dialysate as an index of interstitial ACh concentrations. A dialysis fiber (outer diameter, 310 μm; inner diameter, 200 μm; PAN-1200, 50,000-Da molecular-weight cutoff, Asahi Chemical, Japan) was glued at both ends to polyethylene tubes (length, 25 cm; outer diameter, 500 μm; inner diameter, 200 μm) (Akiyama et al., 1994, Shimizu et al., 2009). The end of the polyethylene tube was enlarged by a dulled needle so that the dialysis fiber could be inserted. The exposed fiber length was 4 mm. The dialysis probe was perfused at a rate of 2 μl/min with Ringer solution containing a cholinesterase inhibitor eserine (100 μM). The amount of ACh in the dialysate was measured using a high-performance liquid chromatography system with electrochemical detection (Eicom, Japan) adjusted to measure low concentrations of ACh (Shimizu et al., 2009).

Two hours after the probe implantation, 10-minute dialysate samples were collected under control conditions, before and during bilateral vagal stimulation (10 V, 1-ms pulse width, 10 Hz). The actual dialysate sampling lagged behind a given collection period by 5 min taking into account the dead space volume between the dialysis membrane and collecting tube. After collecting the control data, the perfusate was replaced with the one containing iberiotoxin (2 μM). The local iberiotoxin administration (Ib_{Local}) is considered to affect vagal nerve terminals in the vicinity of the dialysis fiber. The dose was 40 times higher than that used in the in vitro experimental settings (Pedarzani et al., 2000), taking into account the distribution across the dialysis fiber. According to a previous study in rats (Akiyama et al., 2010), local administration of iberiotoxin at half dose (1 μM) significantly enhanced presynaptic ACh release in response to splanchnic nerve stimulation. Thirty minutes after the initiation of Ib_{Local}, 10-minute dialysate samples were collected before and during bilateral vagal stimulation. Next, iberiotoxin was administered intravenously (0.11 mg/body or 37–48 μg/kg, bolus) while continuing the local iberiotoxin administration. The dose was determined based on a previous study in rats (Meade, 1998) in which intravenous administration of iberiotoxin at approximately half dose (20 μg/kg) significantly blocked BK channels. The local plus intravenous iberiotoxin administration (Ib_{L+IV}) is considered to affect both preganglionic and postganglionic vagal nerve terminals. Ten minutes later, 10-minute dialysate samples were collected before and during bilateral vagal stimulation.

In order to check that a locally administered agent did not reach the vagal ganglia, a supplemental protocol was performed at the end of the experiment in five out of the nine rabbits as follows. The perfusate was replaced with the one containing a ganglionic blocker hexamethonium bromide (100 μM in one rabbit and 1 mM in four rabbits). Thirty minutes later, 10-minute dialysate samples were collected before and during bilateral vagal stimulation.

All data are presented as mean and SE values. Dialysate ACh concentrations were compared among three conditions of control, Ib_{Local} and Ib_{L+IV}, using the Friedman test based on ranks, followed by the rank-sum version of the Student–Newman–Keuls test for all pairwise comparisons (Glantz, 2002). AP and HR were measured just before and at 5 min of the 10-minute bilateral vagal stimulation. The AP and HR data were compared among the three conditions using repeated-measures analysis of variance followed by the parametric version of the Student–Newman–Keuls test (Glantz, 2002). In all of the statistical analyses, differences were considered significant when $P<0.05$.

3. Results

Baseline ACh measured before vagal stimulation did not differ significantly among the three conditions (Fig. 1A, left). Vagal stimulation-induced ACh release was significantly enhanced during the Ib_{Local} ($118\pm5\%$ of the control) and Ib_{L+IV} conditions ($129\pm8\%$ of the control) (Fig. 1A, right). There was no significant difference in the stimulation-induced ACh recovery between the Ib_{Local} and Ib_{L+IV} conditions.

Baseline HR measured before vagal stimulation did not differ significantly among the three conditions (Fig. 1B, left). The stimulation-induced bradycardia was augmented during the Ib_{L+IV} but not the Ib_{Local} conditions compared to the control conditions (Fig. 1B, right).

Baseline AP measured before vagal stimulation did not differ significantly among the three conditions (Fig. 1C, left). AP during vagal stimulation was significantly higher during the Ib_{L+IV} conditions compared to that under the control or Ib_{Local} conditions (Fig. 1C, right).

In the supplemental protocol of local hexamethonium administration, the ACh concentration was 3.3 ± 1.1 nM before vagal stimulation. Bilateral vagal stimulation increased the ACh levels in all of the 5 rabbits to 10.9 ± 7.3 nM ($P<0.05$, one-tailed signed test).

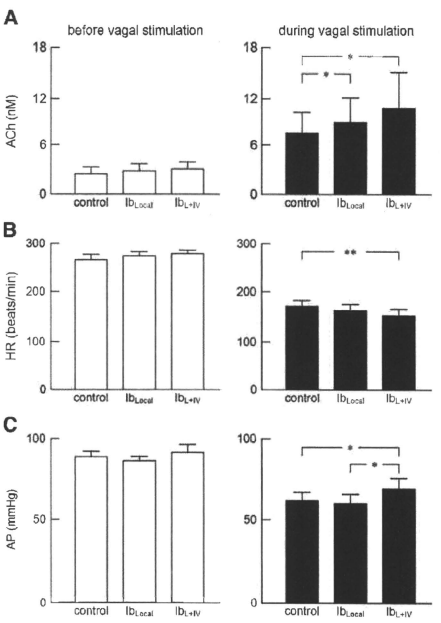

Fig. 1. A: Dialysate acetylcholine (ACh) concentrations under conditions of control, local iberiotoxin administration (Ib_{Local}) and local plus intravenous iberiotoxin administration (Ib_{L+IV}), before (left panel) and during (right panel) bilateral preganglionic vagal stimulation. Ib_{Local} and Ib_{L+IV} significantly increased the vagal stimulation-induced ACh release. B: Heat rate (HR) measured before (left panel) and during (right panel) vagal stimulation. Ib_{L+IV} significantly decreased the HR during vagal stimulation compared to that under control conditions. C: Arterial pressure (AP) measured before (left panel) and during (right panel) vagal stimulation. Ib_{L+IV} significantly increased the AP during vagal stimulation compared to that under the control and Ib_{Local} conditions. Values are mean and mean + SE. *$P<0.05$ and **$P<0.01$.

4. Discussion

Ib_{Local} significantly increased the vagal stimulation-induced ACh release, suggesting that the BK channels play an inhibitory role in the efferent cardiac vagal system (Fig. 1A, right). In a previous study, intravenous administration of hexamethonium bromide completely blocked the vagal stimulation-induced ACh release (Shimizu et al., 2009). In the present study, locally administered hexamethonium bromide is considered to have spread beyond the distribution of locally administered iberiotoxin because of the higher concentration (100 μM or 1 mM vs. 2 μM) and the smaller molecular weight (362.2 vs. 4232.0). Nevertheless, the locally administered hexamethonium bromide did not block the vagal stimulation-induced ACh release, suggesting that the locally administered pharmacological agents failed to reach the vagal ganglia. Therefore, the enhancement of the vagal stimulation-induced ACh release by Ib_{Local} may be attributable to the blockade of the BK channels at the postganglionic vagal nerve terminals.

Under experimental settings similar to the present study, the ACh release at the sinoatrial node can be increased more than 7 times higher during 40-Hz vagal stimulation than during 10-Hz vagal stimulation (Shimizu et al., 2009), suggesting that there remained a sufficient margin for the postganglionic vagal nerve to increase its activity to release ACh when the preganglionic vagal nerve was stimulated at 10 Hz. Under the Ib_{L+IV} conditions, the BK channels are assumed to be blocked at both the preganglionic and postganglionic vagal nerve terminals. If the BK channels limited the preganglionic ACh release to a considerable extent, Ib_{L+IV} could increase the postganglionic vagal nerve activity in response to the preganglionic vagal nerve stimulation. The stimulation-induced ACh release, however, did not differ statistically between the Ib_{Local} and Ib_{L+IV} conditions, suggesting that the inhibitory role of the BK channels at the preganglionic vagal nerve terminals, if any, did not surpass that at the postganglionic vagal nerve terminals.

Although vagi were sectioned at the neck, ACh was detected before vagal stimulation (Fig. 1A, left). In contrast to the vagal stimulation-induced ACh release, the basal ACh release was not affected significantly by Ib_{Local} or Ib_{L+IV}. According to a study using the isolated rat atrium (Abramochkin et al., 2010), a non-quantal ACh release, probably via the choline uptake system, contributes to the basal ACh release from the vagal nerve terminals. It is likely that the blockade of BK channels did not affect the baseline ACh concentrations significantly because the voltage-dependent Ca^{2+} channels contributed little to the basal ACh release.

HR during vagal stimulation under the Ib_{Local} conditions did not differ significantly from that observed under the control conditions (Fig. 1B, right). Presuming that Ib_{Local} affected the ACh release only in the vicinity of the dialysis fiber, not all the vagal nerve fibers innervating the sinoatrial node might have been affected by iberiotoxin. In contrast, HR during vagal stimulation under the Ib_{L+IV} conditions was significantly lower than that observed under the control conditions, suggesting perhaps that the systemically administered iberiotoxin reached a larger portion of the vagal fibers innervating the sinoatrial node.

Ib_{Local} did not affect AP both before and during vagal stimulation (Fig. 1C). Ib_{L+IV} did not increase AP but reduced the vagally mediated hypotension. Possible explanation is as follows. Vagal stimulation significantly decreased AP, possibly via the suppression of cardiac function. Resultantly, the systemic sympathetic system might have been activated through the arterial baroreflex during vagal stimulation. Blockade of the BK channels enhances the vasoconstriction of vascular smooth muscles (Ledoux et al., 2006) and the catecholamine release from the adrenal medulla (Akiyama et al., 2010), resulting in the higher AP during vagal stimulation under the Ib_{L+IV} conditions. The moderation of the vagally mediated hypotension may also have resulted from a more efficient baroreflex response under the Ib_{L+IV} conditions.

There are several limitations in the present study. First, eserine was added to the perfusate to improve the recovery of ACh. Although the inhibition of cholinesterase activity may have affected the ACh kinetics, its influence should have been consistent throughout the protocols. Second, vagal stimulation intensity was selected to limit the hypotensive response and maintain the AP at 60 mm Hg or higher under the control conditions. Based on the results of unilateral vagal stimulation in a previous study (Shimizu et al., 2009), increasing the stimulation frequency would further increase the ACh release. The inhibitory effects of the BK channels on the efferent cardiac vagal system could be different under such an intense vagal stimulation. Finally, the present results do not preclude that the BK channels are on the post-junctional sinus nodal cells or on the cross-inhibitory adrenergic nerves. Nevertheless, the BK channels on the sinus nodal cells or on the adrenergic nerves do not well account for the present results as follows. Although the BK channels on the sinus nodal cells may have modified the HR response and caused possible dissociation between the ACh recovery and the degree of bradycardia, they may not explain the enhanced ACh recovery after the iberiotoxin administration. With respect to the BK channels on the cross-inhibitory adrenergic nerves, if the BK channels are inhibitory to catecholamine release, iberiotoxin is expected to enhance the catecholamine release, antagonizing rather than promoting the vagal ACh release during vagal stimulation. Further studies are needed to confirm these speculations.

In conclusion, blockade of the BK channels by iberiotoxin enhanced the vagal stimulation-induced ACh release and bradycardia, suggesting an inhibitory role of the BK channels in the efferent cardiac vagal system. The inhibitory role of the BK channels at the vagal ganglia did not seem to surpass that at the postganglionic vagal nerve terminals. Although a potential use of selective BK channel openers is expected as vasodilators for vascular smooth muscle dysfunction (Ledoux et al., 2006), there is a possibility that BK channel openers limit vagal effect on the heart, which can be undesirable in certain cardiovascular diseases in which improved vagal function would be helpful.

Acknowledgments

This study was supported by Health and Labour Sciences Research Grants (H18-nano-Ippan-003, H19-nano-Ippan-009, H20-katsudo-Shitei-007, and H21-nano-Ippan-005) from the Ministry of Health, Labour and Welfare of Japan; by a Grant-in-Aid for Scientific Research (No. 20390462) from the Ministry of Education, Culture, Sports, Science and Technology of Japan; and by the Industrial Technology Research Grant Program from the New Energy and Industrial Technology Development Organization (NEDO) of Japan.

References

Abramochkin, D.V., Nurullin, L.F., Borodinova, A.A., Tarasova, N.V., Sukhova, G.S., Nikolsky, E.E., Rosenshtraukh, L.V., 2010. Non-quantal release of acetylcholine from parasympathetic nerve terminals in the right atrium of rats. Exp. Physiol. 95 (2), 265–273.

Akiyama, T., Yamazaki, T., Kawada, T., Shimizu, S., Sugimachi, M., Shirai, M., 2010. Role of Ca^{2+}-activated K^+ channels in catecholamine release from in vivo rat adrenal medulla. Neurochem. Int. 56, 263–269.

Akiyama, T., Yamazaki, T., Ninomiya, I., 1994. In vivo detection of endogenous acetylcholine release in cat ventricles. Am. J. Physiol. 266 (3 Pt 2), H854–H860.

Glantz, S.A., 2002. Primer of Biostatistics, 5th ed. McGraw-Hill, New York.

Ledoux, J., Werner, M.E., Brayden, J.E., Nelson, M.T., 2006. Calcium-activated potassium channels and the regulation of vascular tone. Physiol. 21, 69–79.

Meade, C.J., 1998. The mechanism by which epinastine stops an adenosine analog from contracting BDE rat airways. Am. J. Respir. Crit. Care Med. 157, 522–530.

Pedarzani, P., Kulik, A., Müller, M., Ballanyi, K., Stocker, M., 2000. Molecular determinants of Ca^{2+}-dependent K^+ channel function in rat dorsal vagal neurones. J. Physiol. 527, 283–290.

Shimizu, S., Akiyama, T., Kawada, T., Shishido, T., Yamazaki, T., Kamiya, A., Mizuno, M., Sano, S., Sugimachi, M., 2009. In vivo direct monitoring of vagal acetylcholine release to the sinoatrial node. Auton. Neurosci. 148, 44–49.

Experimental Physiology – *Research Paper*

Dynamic characteristics of heart rate control by the autonomic nervous system in rats

Masaki Mizuno[1,2], Toru Kawada[2], Atsunori Kamiya[2], Tadayoshi Miyamoto[2,3], Shuji Shimizu[2], Toshiaki Shishido[2], Scott A. Smith[1] and Masaru Sugimachi[2]

[1]*Departments of Physical Therapy and Internal Medicine, University of Texas Southwestern Medical Center at Dallas, TX, USA*
[2]*Department of Cardiovascular Dynamics, National Cerebral and Cardiovascular Center Research Institute, Osaka, Japan*
[3]*Department of Physical Therapy, Morinomiya University of Medical Sciences, Osaka, Japan*

We estimated the transfer function of autonomic heart rate (HR) control by using random binary sympathetic or vagal nerve stimulation in anaesthetized rats. The transfer function from sympathetic stimulation to HR response approximated a second-order, low-pass filter with a lag time (gain, 4.29 ± 1.55 beats min^{-1} Hz^{-1}; natural frequency, 0.07 ± 0.03 Hz; damping coefficient, 1.96 ± 0.64; and lag time, 0.73 ± 0.12 s). The transfer function from vagal stimulation to HR response approximated a first-order, low-pass filter with a lag time (gain, 8.84 ± 4.51 beats min^{-1} Hz^{-1}; corner frequency, 0.12 ± 0.06 Hz; and lag time, 0.12 ± 0.08 s). These results suggest that the dynamic characteristics of HR control by the autonomic nervous system in rats are similar to those of larger mammals.

(Received 5 March 2010; accepted after revision 24 May 2010; first published online 28 May 2010)
Corresponding author M. Mizuno: Department of Physical Therapy, University of Texas Southwestern Medical Center at Dallas, 5323 Harry Hines Boulevard, Dallas, TX 75390-9174, USA. Email: masaki.mizuno@utsouthwestern.edu

Despite extensive use of rats in cardiovascular research, the dynamic characteristics of heart rate (HR) control by the autonomic nervous system in this species remain to be elucidated. To better understand the autonomic control of HR in rats, it is important to quantitatively assess the input–output relationship between autonomic nerve stimulation and HR over a wide range of frequencies that are of physiological interest. By understanding these relationships in the rat, data obtained using this animal model may be more readily extrapolated to larger mammals, including humans.

Heart rate variability is considered to reflect autonomic tone because its components change both physiologically (e.g. standing and ageing) and pathophysiologically (e.g. hypertension and heart failure; Malliani *et al.* 1991). Based on dog and human studies, the very low-frequency (VLF) component (0.02–0.08 Hz) is likely to reflect changes in vasomotor tone in relation to thermoregulation and local adjustment of resistance in individual vascular beds; the low-frequency (LF) component (0.08–0.15 Hz) is considered to be Mayer's wave and a marker of sympathetic activity; and the high-frequency (HF) component (0.15–0.40 Hz) mainly originates from respiratory activity and is considered to be mediated by vagal activity (Pagani *et al.* 1986). Based on the differences in HR spectra between conscious rats and rats in which autonomic blockade was induced pharmacologically, Cerutti *et al.* (1991) determined that the VLF component ranged between 0.017 and 0.26 Hz, the LF component ranged between 0.27 and 0.74 Hz, and the HF component was above 0.75 Hz. Even though these allocations in frequency band in rats corresponded to their considerably higher basal HR (range between 300 and 400 beats min^{-1}) compared with that of larger mammals, such as dogs and humans (range between 60 and 100 beats min^{-1}), there has been no scientific rationale provided for setting these allocations. This is because it is unknown whether the dynamic characteristics of HR control by the autonomic nervous system in rats are significantly different from those in larger mammals, such as rabbits (Kawada *et al.* 1996), cats (Chess & Calaresu, 1971) and dogs (Berger *et al.* 1989).

Given that the release and disposition of neurotransmitters (e.g. noradrenaline and acetylcholine) at autonomic nerve endings may be determined biochemically, regardless of body size, we hypothesized that the dynamic characteristics of HR control by the autonomic nervous system would not differ appreciably among different mammalian species. To test this

DOI: 10.1113/expphysiol.2010.053090

hypothesis, we quantified the dynamic characteristics of HR control mediated by sympathetic or vagal nerve stimulation in rats using transfer function analysis. The results provide the first quantitative data on the dynamic characteristics of autonomic HR regulation in rats. Since HR changes dynamically in response to daily activities, quantification of how quickly the HR can respond to sympathetic or vagal nerve stimulation is important. For instance, information on the dynamic HR response is key to understanding the generation of HR variability. The present study aims to expand our knowledge of HR control by the autonomic nervous system.

Methods

Surgical preparation

Animal care was in accordance with the *Guiding Principles for Care and Use of Animals in the Field of Physiological Sciences*, approved by the Physiological Society of Japan. All protocols were reviewed and approved by the Animal Subjects Committee of the National Cerebral and Cardiovascular Center. Thirteen Sprague–Dawley rats (body weight, 340–670 g) were anaesthetized using a mixture of urethane (250 mg ml^{-1}; Sigma, St. Louis, MO, USA) and α-chloralose (40 mg ml^{-1}; Sigma), initiated with an intraperitoneal bolus injection of 1 ml kg^{-1}. If additional anaesthesia was needed, 0.1 ml kg^{-1} was given intraperitoneally. The rats were intubated and mechanically ventilated with oxygen-enriched room air. The rats were slightly hyperventilated to suppress chemoreflexes (arterial P_{CO_2} ranged from 30 to 35 mmHg; arterial P_{O_2} > 300 mmHg). Arterial blood pH was within the physiological range. A catheter was placed in the right femoral artery, which was connected to a pressure transducer (DX-200, Nihon Kohden, Tokyo, Japan) to measure arterial pressure (AP). Heart rate was measured using a cardiotachometer (AT601G, Nihon Kohden, Tokyo, Japan) triggered by the R wave on the electrocardiogram. The HR series were checked by visual inspection. A catheter was introduced into the right femoral vein for drug administration. Sino-aortic denervation was performed bilaterally to minimize changes in the sympathetic efferent nerve activity via arterial baroreflexes. The vagi were sectioned bilaterally at the neck. A pair of bipolar stainless-steel electrodes was attached to the right cervical sympathetic nerve for efferent sympathetic stimulation or the right cervical vagus for efferent vagal stimulation. The stimulation electrodes and nerve were secured with silicon glue (Kwik-Sil, World Precision Instruments, Sarasota, FL, USA). Body temperature was monitored with a thermometer placed in the rectum, and was maintained at 38°C with a heating pad throughout the experiment.

Experimental procedures

The pulse duration was set at 2 ms and the stimulation amplitude was fixed at 10 V for both sympathetic and vagal nerve stimulation. To allow stable haemodynamics, sympathetic and vagal nerve stimulation was started at ~1 h after the end of surgical preparation. Between sympathetic and vagal stimulation protocols, >15 min elapsed to allow AP and HR to return to their respective baseline values.

To estimate the dynamic transfer characteristics from sympathetic stimulation to the HR response, the sectioned end of the right cervical sympathetic nerve was stimulated, employing a frequency-modulated pulse train for 10 min. The stimulation frequency was switched every 1000 ms to either 0 or 5 Hz, according to a binary white-noise signal. The power spectrum of the stimulation signal was reasonably constant up to 0.5 Hz. The transfer function was estimated up to 0.5 Hz because the reliability of estimation decreased owing to the diminution of input power above this frequency. The selected frequency range was determined based on previous results in rabbits (Kawada *et al.* 1996) so that it would sufficiently span the physiological range of interest with respect to the dynamic sympathetic control of HR.

To estimate the dynamic transfer characteristics from vagal stimulation to the HR response, the right vagus was stimulated, employing a frequency-modulated pulse train for 10 min. The stimulation frequency was switched every 500 ms to either 0 or 10 Hz, according to a binary white-noise signal. The power spectrum of the stimulation signal was reasonably constant up to 1 Hz. The transfer function was estimated up to 1 Hz because the reliability of estimation decreased owing to the diminution of input power above this frequency. The selected frequency range was determined based on previous results in rabbits (Kawada *et al.* 1996) so that it would sufficiently span the physiological range of interest with respect to the dynamic vagal control of HR.

The switching intervals differed between sympathetic and vagal stimulation for the following reasons. In theory, the switching interval of binary white noise is inversely related to an upper frequency bound for the input modulation frequency. Prior knowledge in rabbits (Kawada *et al.* 1996) and preliminary results in rats indicated that the upper frequency bound of physiological interest might be lower for the sympathetic transfer function, which rendered the switching interval longer for the sympathetic stimulation. Another reason relates to the stimulation frequency. In the present study, the sympathetic stimulation frequency of 5 Hz and the vagal stimulation frequency of 10 Hz were determined based on the HR response. Once the stimulation frequency is determined, there is a methodological limitation for setting the switching interval. For example, a switching

interval of 500 ms is too close to a pulse interval of 200 ms (i.e. 5 Hz stimulation). In this case, only two pulses can be applied in the shortest interval of 500 ms, which means that the stimulation frequency may be in effect 4 Hz rather than the intended 5 Hz. This problem does not occur with a 1000 ms switching interval in combination with 5 Hz stimulation and 500 ms switching interval in combination with 10 Hz stimulation.

Background sympathetic tone is known to augment vagal HR control (an accentuated antagonism; Levy, 1971; Kawada *et al.* 1996). To eliminate any effect of sympathetic activity, in seven out of the thirteen rats the vagal stimulation protocol was repeated after the administration of the β-adrenergic blocker propranolol (1 mg kg^{-1} I.V.; Perlini *et al.* 1995).

Data analysis

Data were digitized at 200 Hz using a 12 bit analog-to-digital converter and stored on the hard disk of a dedicated laboratory computer system. The dynamic transfer function from binary white-noise stimulation to the HR response was estimated based on the following procedure. To avoid the possibility that the initial transition from no stimulation to random stimulation biased the transfer function estimation, data were processed only from 2 min after the initiation of random stimulation. Input–output data pairs of the stimulation frequency and HR were resampled at 10 Hz. Subsequently, data pairs were partitioned into eight 50%-overlapping segments consisting of 1024 data points each. For each segment, the linear trend was subtracted and a Hanning window was applied. A fast Fourier transform was then performed to obtain the frequency spectra of nerve stimulation [$N(f)$] and HR [$HR(f)$]. Over the eight segments, the power of the nerve stimulation [$S_{N\cdot N}(f)$], the power of the HR [$S_{HR\cdot HR}(f)$], and the cross-power between these two signals [$S_{N\cdot HR}(f)$] were ensemble averaged. Finally, the transfer function [$\mathrm{H}(f)$] from nerve stimulation to the HR response was determined using the following equation (Marmarelis & Marmarelis, 1978):

$$\mathrm{H}(f) = \frac{S_{N\cdot HR}(f)}{S_{N\cdot N}(f)} \quad (1)$$

To quantify the linear dependence of the HR response on vagal or sympathetic stimulation, the magnitude-squared coherence function [$\mathrm{Coh}(f)$] was estimated by employing the following equation (Marmarelis & Marmarelis, 1978):

$$\mathrm{Coh}(f) = \frac{|S_{N\cdot HR}(f)|^2}{S_{N\cdot N}(f) \times S_{HR\cdot HR}(f)} \quad (2)$$

Coherence values range from zero to unity. Unity coherence indicates perfect linear dependence between the input and output signals; in contrast, zero coherence indicates total independence between the two signals.

As preliminary results suggested that the transfer function from sympathetic stimulation to HR response in rats approximated a second-order low-pass filter with pure delay, as in the case of rabbits (Kawada *et al.* 1996, 2009), we determined the parameters of the sympathetic transfer function using the following equation:

$$\mathrm{H}(f) = \frac{K}{1 + 2\zeta\frac{f}{f_N}j + \left(\frac{f}{f_N}j\right)^2} e^{-2\pi f j L} \quad (3)$$

where K is dynamic gain (in beats per minute per herz), f_N is the natural frequency (in herz), ζ is the damping ratio, L is lag time (in seconds), and f and j represent frequency and imaginary units, respectively. The dynamic gain (K, in beats per minute per herz) represents the asymptotic value of transfer gain as the frequency approaches zero, and corresponds to the steady-state response in the step response. The natural frequency (f_N, in herz) determines the frequency limit of the low-pass filter above which the transfer gain reduces as the frequency increases. In the second-order low-pass filter, the maximal negative slope of the gain diminution is 1/100 per 10 Hz. The damping ratio (ζ, unitless) characterizes how the transfer gain varies around the f_N. The lag time (L, in seconds) indicates the latency of signal transmission from nerve stimulation to the initiation of HR response. These parameters were estimated by means of an iterative non-linear least-squares regression.

As preliminary results suggested that the transfer function from vagal stimulation to HR response in rats approximated a first-order low-pass filter with pure delay, as in the case of rabbits (Kawada *et al.* 1996, 2009), we determined the parameters of the vagal transfer function using the following equation:

$$\mathrm{H}(f) = \frac{-K}{1 + \frac{f}{fc}j} e^{-2\pi f j L} \quad (4)$$

where K represents the dynamic gain (in beats per minute per herz), fc denotes the corner frequency (in herz), L denotes the lag time (in seconds), and f and j represent frequency and imaginary units, respectively. The negative sign in the numerator indicates the negative HR response to vagal stimulation. The dynamic gain (K, in beats per minute per herz) represents the asymptotic value of transfer gain as the frequency approaches zero. The corner frequency (fc, in herz) represents the frequency at which the transfer gain decreases by 3 dB relative to K. Higher fc indicates the more rapid HR response to vagal stimulation. In the first-order low-pass filter, the maximal slope of the gain diminution is 1/10 per 10 Hz. The lag time (L, in seconds) indicates the latency of signal transmission from nerve stimulation to the initiation of HR response. These

parameters were estimated by means of an iterative non-linear least-squares regression.

To facilitate the intuitive understanding of the system's dynamic characteristics, we calculated the system step response of HR to 1 Hz nerve stimulation as follows. The system impulse response was derived from the inverse Fourier transform of $H(f)$. The system step response was then obtained from the time integral of the impulse response. The length of the step response was 51.2 s. The 80% rise time for sympathetic step response or the 80% fall time for vagal step response was estimated at the time which the step response reached 80% of the steady-state response, calculated by averaging the last 10 s of data from the step response.

Statistical analysis

All data are represented as means ± S.D. Student's paired *t* test was used to test differences in haemodynamic parameters. In seven rats, parameters of vagal transfer function were compared before and after propranolol administration using Student's paired *t* test. Values of $P < 0.05$ were considered significant.

Results

Typical recordings

Figure 1 shows typical recordings of sympathetic and vagal stimulation obtained from one rat. While HR varied immediately during random vagal stimulation, it changed only gradually during random sympathetic stimulation. Sympathetic stimulation increased the mean HR from 375.5 ± 33.5 to 444.9 ± 28.4 beats min^{-1} ($P < 0.05$); vagal stimulation decreased the mean HR from 378.2 ± 31.9 to 317.3 ± 47.1 beats min^{-1} ($P < 0.05$). Neither sympathetic nor vagal stimulation altered mean AP (79.1 ± 18.4 *versus* 75.1 ± 19.4 and 78.2 ± 20.2 *versus* 72.4 ± 18.3 mmHg, respectively).

Sympathetic transfer function

Figure 2*A* illustrates the dynamic transfer function characterizing sympathetic HR control averaged from all animals. Gain plots, phase plots and coherence functions are shown. The sympathetic transfer function approximated a second-order, low-pass filter with a lag time (dynamic gain, 4.29 ± 1.55 beats min^{-1} Hz^{-1}; natural frequency, 0.07 ± 0.03 Hz; damping coefficient, 1.96 ± 0.64; and lag time, 0.73 ± 0.12 s). Figure 2*B* shows the calculated step response of HR to sympathetic stimulation averaged from all animals. As expected, sympathetic stimulation gradually increased HR. The steady-state sympathetic response was 3.86 ± 1.80 beats min^{-1} Hz^{-1}. The 80% rise time for the sympathetic step response was 13.7 ± 5.1 s.

Vagal transfer function

Figure 2*C* illustrates the dynamic transfer function characterizing vagal HR control averaged from all animals. The vagal transfer function approximated a first-order, low-pass filter with a lag time (dynamic gain, 8.84 ± 4.51 beats min^{-1} Hz^{-1}; corner frequency, 0.12 ± 0.06 Hz; and lag time, 0.12 ± 0.08 s). Figure 2*D* shows the calculated step response of HR to vagal

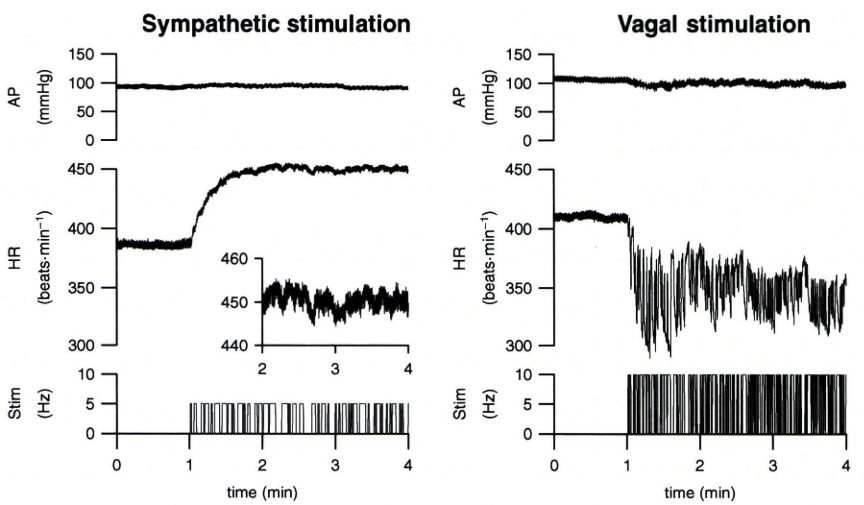

Figure 1. Raw trace of 10 Hz resampled arterial pressure (AP; top) and heart rate (HR; middle) obtained using binary white-noise stimulation (Stim; bottom)
Recordings are shown for sympathetic (left) and vagal nerve stimulation (right). The inset in the panels for sympathetic stimulation indicates the expanded ordinate for the HR response.